AIP | The Journal of Chemical Physics

Temperature inhomogeneities simulated with multiparticle-collision dynamics

Daniel Lüsebrink and Marisol Ripoll

Citation: J. Chem. Phys. **136**, 084106 (2012); doi: 10.1063/1.3687168
View online: http://dx.doi.org/10.1063/1.3687168
View Table of Contents: http://jcp.aip.org/resource/1/JCPSA6/v136/i8
Published by the American Institute of Physics.

Temperature inhomogeneities simulated with multiparticle-collision dynamics

Daniel Lüsebrink and Marisol Ripoll[a)]
Theoretical Soft-Matter and Biophysics, Institute of Complex Systems, Forschungszentrum Jülich, 52425 Jülich, Germany

(Received 28 October 2011; accepted 2 February 2012; published online 27 February 2012)

The mesoscopic simulation technique known as multiparticle collision dynamics is presented as a very appropriate method to simulate complex systems in the presence of temperature inhomogeneities. Three different methods to impose the temperature gradient are compared and characterized in the parameter landscape. Two methods include the interaction of the system with confining walls. The third method considers open boundary conditions by imposing energy fluxes. The transport of energy characterizing the thermal diffusivity is also investigated. The dependence of this transport coefficient on the method parameters and the accuracy of existing analytical theories is discussed. © *2012 American Institute of Physics*. [http://dx.doi.org/10.1063/1.3687168]

I. INTRODUCTION

The influence of temperature inhomogeneities is of high relevance for many systems in nature and industry. Examples range from separation techniques,[1,2] microfluidic applications,[3,4] or even conditions that might have facilitated the origin of life.[5,6] The physical phenomena related with the presence of temperature gradients are *thermophoresis* or transport of mass, and transport of energy. Apart from various experimental techniques,[7] and analytical theories,[8,9] the development of computers and simulation techniques has already contributed to gain deeper understanding and to increase the applicability of these phenomena.[10–12]

A large part of the existing simulations that consider the presence of temperature gradients are performed with molecular dynamics (MD) with essentially an atomistic description of the system,[13–15] or alternatively with direct simulation Monte Carlo method (DSMC), which is a particle-based, numerical scheme for solving the nonlinear Boltzmann equation for hard spheres.[16–18] Nevertheless, reproducing the properties of most soft matter systems such as colloidal dispersions or polymer solutions is a task beyond the possibilities of simulations based in these approaches. The large separation of the relevant length and time scales of solute and solvent requires the formulation of effective coarse-grained descriptions of the solvent and the solute. An important requirement of such descriptions is the inclusion of *hydrodynamic interactions* which are mediated by the solvent and are non-local both in time and space. In recent years, several particle-based hydrodynamic mesoscopic techniques have been proposed.[19] Mass and momentum local conservation are necessary requirements for hydrodynamic interactions to be correctly modeled. Two of the most well-known and extended hydrodynamic mesoscopic simulation techniques are lattice Boltzmann (LB) (Refs. 20, 21) and dissipative dynamics dynamics (DPD).[22–24] In the most extended versions of both these methods mass and momentum are locally conserved quantities but not the energy, what means that they are restricted to be used in isothermal conditions. In the LB method particle densities move in the nodes of a lattice with discretized velocities, such that mass and momentum fulfil local conservation laws.[21] In order to include the internal energy flux several routes have been explored[25–28] without one that has clearly shown to be the optimal one. Examples are to consider higher complexity of the lattices to increase the symmetries, to add counter-terms to cancel spurious anisotropic operators, or to account for hybrid descriptions. These approaches have recently been successfully employed to investigate systems such as phase separation of binary fluids[29] or Rayleigh Taylor instabilities.[30] In standard DPD, particles positions and velocities are updated according to Newton equations of motion by considering conservative, dissipative, and stochastic interactions. Mass and momentum are then conserved quantities and thermal fluctuations are taken into account. An energy conserving extension of the method (DPD+e) has been proposed[31,32] by considering an internal energy variable for each particle, where only the heat conduction contribution needs to be specified.[33–35] It has been shown that DPD+e can sustain transport of energy and temperature gradients,[33,36,37] although precise conservation requires integration algorithms even more involved than in standard DPD.[38–40] Recent applications of this model have been found in convection,[41] multicomponet systems,[42] and nanocomposities.[43]

A more recent approach has been proposed by Malevanets and Kapral[44,45] with the method multiparticle collision dynamics (MPC), also known as stochastic rotation dynamics. This method conserves in its basic implementation mass, momentum, and energy, including also thermal fluctuations. This simplicity presents MPC as a promising tool for the investigation of the effect of temperature inhomogeneities in complex systems. In this work, we include essentially for the first time temperature gradients with the MPC method, carefully analyzing the implementation in confinement and with open boundary conditions.[46] We also investigate the transport of heat characterizing the thermal diffusivity coefficient as a function of the MPC parameters.

[a)]Electronic mail: m.ripoll@fz-juelich.de.

II. METHOD

A. Multiparticle collision dynamics

MPC is a particle-based method, in which the solvent is represented by N point particles.[47,48] Each particle $i = (1, \ldots, N)$ has a constant mass m_i, a variable position $\mathbf{r}_i$, and a variable velocity $\mathbf{v}_i$. The mass of the particles is typically the same for all of them m, while positions and velocities are continuously distributed in the phase space. The MPC dynamics takes place in two alternating steps. In the *streaming step* all particles ballistically propagate ignoring their neighbours during a certain collision time h,

$$\mathbf{r}_i(t+h) = \mathbf{r}_i(t) + h\mathbf{v}_i(t). \tag{1}$$

In the *collision step* the simulation box is divided in cubic collision boxes of size a. The interaction is performed among particles in the same collision box through the center of mass velocity $\mathbf{v}_{cm,\,i}$ that considers all particles j which are located in the same collision box as particle i at time t,

$$\mathbf{v}_{cm,i}(t) = \frac{\sum_j^{i,t} m_j \mathbf{v}_j(t)}{\sum_j^{i,t} m_j}. \tag{2}$$

The actual collision is defined as a rotation by an angle α around a random direction of the relative velocity of the particle to the collision box center of mass. The particle velocity after the collision is then,

$$\mathbf{v}_i(t+h) = \mathbf{v}_{cm,i}(t) + \mathcal{R}(\alpha)[\mathbf{v}_i(t) - \mathbf{v}_{cm,i}(t)], \tag{3}$$

with $\mathcal{R}(\alpha)$ the stochastic rotation matrix. This simple collision rule implies that each particle changes the magnitude and the direction of its velocity, such that the total mass, momentum, and also kinetic energy are conserved in each collision box before and after the collision. This ensures the presence of hydrodynamic interactions, together with the sustainability of temperature gradients, and thermal fluctuations. In order to preserve Galilean invariance, and to enhance collisional transport *random shift* needs to be additionally considered.[49] This simply means that the superimposed regular lattice that defines the collision boxes has an origin that shifts in each collision between 0 and a in each direction.

The reference units are usually chosen to be the particle mass m, the collision box size a, and the equilibrium temperature T, that are typically set to one. This corresponds to measure length as $\hat{x} = x/a$ and time as $\hat{t} = t\sqrt{k_B T/ma^2}$, with k_B the Boltzmann constant. The parameters that will determine the properties of the MPC are then the collision time h, the rotation angle α, and the number particle density $\rho = Na^3/V$, with V the volume of the simulation box. The range of parameters with large values of α and small values of h has shown to display a liquid-like behavior characterized by large values of the Schmidt number $Sc = \nu/D$ with ν the kinematic viscosity and D the diffusion coefficient.[50,51] Local angular momentum conservation is though violated in this standard formulation. An appropriate modification of the method has already been proposed,[52,53] for cases in which this is of relevance.

The MPC method has already been extensively tested, showing, for example, to reproduce the Navier-Stokes equation,[44] to include hydrodynamic interactions in polymer solutions,[50,54] or more recently to fulfil the fluctuation theorem.[55] In isothermal conditions, MPC has already been applied to a large number of systems like colloidal solutions,[56,57] rod-like colloids,[58,59] polyelectrolyte solutions,[60] or nanoswimmers.[61–63]

B. Temperature profile establishment

We simulate a three-dimensional system, with periodic boundary conditions in two spatial directions, and a temperature difference imposed at the boundaries of the third direction, z. The boundary temperatures are T_c at the cold bath, and T_h at the hot bath (with $T_c < T_h$). Various possible implementations of the thermal baths are discussed in Sec. III. For clarity, we explain before some general aspects of the temperature profile establishment. Initially the system has a uniform temperature, which is generally chosen to be $T_0 = (T_h + T_c)/2$. After a short equilibration time, the system in contact with the thermal baths displays a steady temperature distribution that for not too large temperature differences is linear,

$$T(z) = T_c + \frac{T_h - T_c}{L_z} z, \tag{4}$$

with L_z the distance between the two baths. An example of the simulated temperature profile can be seen in Fig. 1, with $L_z = L_y = L_x = 40$. The temperature is computed as the average kinetic energy per particle, with averages calculated within layers parallel to the walls and therefore perpendicular to the temperature gradient direction. The actual average system temperature shows small deviations from T_0 in the case that the total energy is not a fixed quantity, when it will be time dependent $\langle T(t) \rangle$. In these cases, all particle velocities can globally be rescaled to enforce precisely this constraint, with a frequency to be determined in each application. We choose as the reference value $\overline{T} = 1$, the average temperature in absence of fluctuations, namely, T_0. Standard values chosen for the boundary temperatures are $T_c = 0.9$ and $T_h = 1.1$. These values result in a relative temperature difference $(T_h - T_c)/\overline{T} = 0.2$. Considering as a reference value the room temperature $\overline{T} = 300$ K, this relative difference would correspond to a temperature difference of 60 °C.

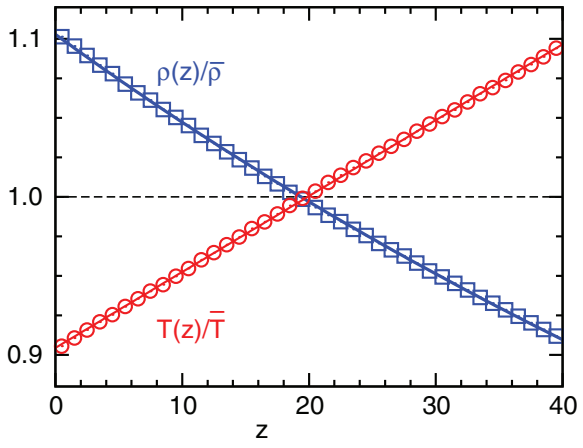

FIG. 1. Example of a temperature profile (circles) and the corresponding particle number density profile (squares). The symbols report the simulated values and the lines correspond respectively to Eqs. (4) and (5).

Together with the temperature profile, the solvent density also becomes position dependent as a result of a constant pressure p throughout the system. The MPC fluid is known to behave with the ideal gas equation of state, $pV = Nk_BT$. The position dependent particle number density $\rho(z) = N(z)a^3/V$ is then,

$$\rho(z) = \frac{p}{k_B T(z)}. \tag{5}$$

If the temperature profile in Eq. (4) is considered, the pressure can be calculated taking into account that the total number of particles in the simulation box is constant, i.e., $\int_V d^3r\rho(z) = N$, what leads to

$$p = \rho \frac{k_B(T_h - T_c)}{\ln(T_h/T_c)}. \tag{6}$$

Although Eq. (5) corresponds to a inversely linear dependence with the position, in the limit of small temperature differences, the density profile can be approximated to a linear function,

$$\rho(z) = \rho\left[1 - \frac{1}{\overline{T}}\frac{T_h - T_c}{L_z}\left(z - \frac{L_z}{2}\right)\right] \tag{7}$$

as can be seen in Fig. 1.

III. BOUNDARY CONDITIONS

A. Walls with virtual particles

Systems confined between parallel walls at homogeneous temperature conditions have been largely simulated with the MPC solvent.[64–66] In order to obtain stick boundary conditions, i.e., walls and neighbouring particles with equal velocities, two modifications have been included in the algorithm. First in the streaming step bounce-back is considered. This means that particles reaching one of the walls revert their direction and velocity. In the collision step the consideration of random shift translates in partially filled collision boxes at the walls, such that the effect of virtual particles is considered.[64] In cases where there are n_w interacting particles in a collision box intersecting with the wall with $n_w < \rho$, $\rho - n_w$ virtual particles will be considered. These particles are chosen with a momenta drawn from a Maxwell-Boltzmann distribution with zero mean velocity and variance $(\rho - n_w)\sqrt{k_B\overline{T}/m}$, such that the values for temperature and density match those values in the bulk.

The implementation of the temperature gradient is achieved by considering the walls as thermal baths and imposing temperatures T_c and T_h, respectively, in the cold and hot walls. The corresponding densities ρ_c and ρ_h are then given by Eq. (5). Therefore, the interaction with the virtual particles in the hot wall provides energy to the system, while the interaction with the virtual particles in the cold wall absorbs averagely an equivalent amount of energy. The temperature distribution of the solvent between the walls nicely reaches a linear profile. The temperature of the fluid close to the walls is though not the same as the wall temperature as can be seen in Fig. 2(a). This temperature jump is an effect related although decoupled to the slip velocity of particles close to a wall in the presence of solvent flow.[67,68] In order to characterize the temperature jump, we define the dimensionless quantity T_J,

$$T_J = \frac{T(0) - T_c}{\overline{T} - T_c}. \tag{8}$$

The solvent temperatures at the walls, $T(0)$ and $T(L_z)$ can be characterized from a linear fit. In case of perfect match $T(0) = T_c$, and $T_J = 0$ by construction. Meanwhile, in the limiting case of maximum mismatch, there would be no temperature variation upon contact with the heat bath, this is $T(0) = \overline{T}$ and $T_J = 1$.

Figure 2(b) shows T_J as a function of the solvent parameters, that increases for decreasing α and increasing h. The dependence of T_J with the system size is further analyzed for a parameter set with large temperature mismatch values. Results are displayed in Fig. 2(c) where it can be seen that

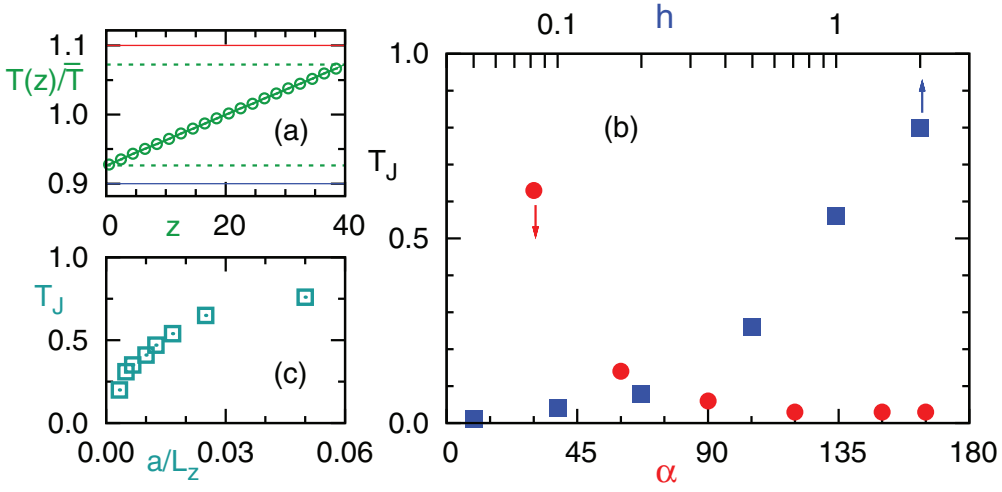

FIG. 2. (a) Temperature profile with $h = 0.5$ and walls with virtual particles. Open circles are simulation results, solid lines are the temperatures imposed at the walls, and dashed lines the actual boundary temperatures $T(0)$ and $T(L_z)$. Otherwise stated the employed parameters are $h = 0.1$, $\alpha = 120$, $\rho = 5$, a cubic size $L = 40$, $T_c = 0.9$, and $T_h = 1.1$. (b) Dimensionless temperature jump T_J in Eq. (8) as a function of α (circles, down-axis), and as a function of h (squares, up-axis). (c) Dependence of T_J with the inverse of the system length L_z in the temperature gradient direction, with $\alpha = 30$ and $L_x = 20 = L_y$.

increasing L_z noticeable decreases T_J. Eventually, it can be extrapolated that $T_J \to 0$ for $L_z \to \infty$. On the other hand, we have checked that T_J does not depend on the neutral directions L_x, L_y, and no significant differences are observed by choosing the hot layer instead of the cold in the definition of T_J in Eq. (8). Finally, trial simulations imposing a starting configuration with $T_J = 0$, show the same final stationary state with $T_J \neq 0$.

Similar effects have already been observed in simulations performed with other methods as DSMC (Ref. 17) or LB,[69,70] and are known in the context of rarefied gases.[67,68] The common physical characteristic in these systems is that the average particle mean free path λ varies due to the presence of the wall, such that it is effectively smaller in the neighbourhood of a wall than in the bulk region. Considering this variation, kinetic theory predicts the existence of a layer of width λ with nonlinear temperature profile,[67,68] what defines the *kinetic boundary layer*, also known as the *Knudsen layer*. The overall relevance of such layer effect is then related with the system size, via the *Knudsen number* which is defined as $Kn = \lambda/L$ being L a characteristic system size, which in our case is the distance between walls L_z. The mean free path in MPC is usually defined as $\lambda = h\sqrt{k_B T/m}$. This is though not an appropriate value to quantify Kn, since a more physical definition should regard the increase of λ with decreasing collision angle,[71] and decreasing density, what would account for the divergence in the limit $\alpha \to 0$, or $\rho \to 0$, where no collisions occur. All our results in Figs. 2(b) and 2(c) could then be explained as direct relation between of T_J and Kn similar to the behavior of rarefied gases.[67,68] A small difference could have been expected by choosing the hot layer in the definition of T_J in Eq. (8) since the width of the Knudsen layer depends on the temperature. It seems though that the differentiation is smaller than the statistical precision of the presented simulation results.

In the DPD-heat conduction model[33,34] arrested particles interchange internal energy, such that in spite of the absence of particle motion, local temperature variations are possible. Simulations with this model have shown to display a temperature gradient without any jump in the proximity of the walls. This observation also supports the explanation of the MPC temperature jump at the walls in terms of the variation of the Knudsen number. A different system where a surface temperature drop has been experimentally observed is a strongly heated spherical nanoparticle in a thermalized fluid.[72] In this case, the fluid has radially varying temperature around the particle which displays a jump relative to the particle temperature. This has been justified as a manifestation of the interfacial thermal resistance, caused by the mismatch of the thermal properties between the solid and liquid, and by the strength of the interfacial bonding, although the dependence of the Knudsen number has not been yet analyzed.

B. Walls with thermostats

To investigate other routes that more accurately accommodate the temperature of the solvent particles close to the walls, we disregard the virtual particles at the walls, and implement thermostats in the boundary slabs next to the walls. The limiting temperatures T_c and T_h are now enforced in the cells neighbouring the walls by rescaling the kinetic energies of such solvent particles in each simulation step. The temperature distribution is now linear sufficiently far away from the walls as can be seen in the inset of Fig. 3. A shoulder-like behavior appears though close to the boundaries, what implies the presence of a temperature jump. To quantify this behavior, we employ the definition of T_J in Eq. (8) with $T(0)$ calculated from a linear fit to the temperature profile by excluding the first slabs at the boundaries, as shown in the inset of Fig. 3. Similarly to the previous case, T_J is dependent on the method parameters, as shown in Fig. 3. As it could be expected, the data show a similar trend, and T_J becomes more significant for large values of h or smaller α given a certain value of the system size. This is in agreement with the dependence of the Knudsen number. The deviation of the wall temperature is though much less pronounced than for the virtual particles in Fig. 2(b). It can therefore be concluded that the dependence of the temperature jump does not only depend exclusively on the Knudsen number but also on the specific boundary conditions that provide different energy accommodation coefficients.[68]

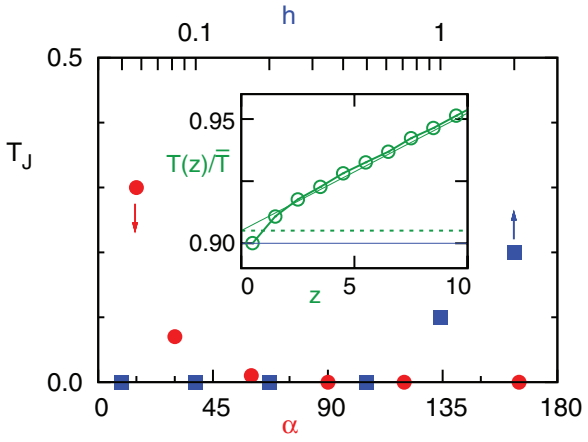

FIG. 3. T_J for walls with thermostats as a function of α, and h. Symbols and parameters similar to Fig. 2. The inset shows the detail of a temperature profile close to the wall for with $\alpha = 30$, $h = 0.1$, $\rho = 5$, and $L_z = 40$.

1. Comparison of wall implementations

We can conclude that both these methods produce satisfactory linear profiles away from the walls, apart from the temperature jump at the boundaries. Therefore, they can be employed to study the effects of temperature gradients in the presence of confining walls. Furthermore, the parameters for which the temperature jump are smallest, namely, small collision times h, and large α values, are the parameters for which the MPC algorithm has been mostly employed, since they are also the values for which the Schmidt number is larger and where MPC behaves as a liquid-like solvent.[50,51,54]

In order to compare the two methods for implementing walls at different temperatures, several issues have to be considered. First, we have characterized that the temperature jump is considerably more pronounced for the walls with virtual particles than for the thermostat ones. In practice, the

effective temperature gradient will be calculated with the actual boundary temperatures, and given that in both cases the profiles are nicely linear, no further consequences are expected unless the precise boundary behavior is of interest. From the computational point of view, it should be noted that virtual particles at the walls constitute an additional, but not really significant effort since just three stochastic velocities per collision box are required. This computational cost is approximately the same as the thermalization of the layers in the proximity of the wall. With both techniques the boundary layers have to be disregarded. In the case of the virtual particles one layer will be sufficient, while for the thermostated walls it will be necessary to not account for at least two layers. Consequently, the walls with virtual particles will be in general better suited to study temperature gradients in the presence of confining walls, although a more precise consideration should be performed in each particular application of the methods.

C. Periodic boundary conditions: Velocity exchange algorithm

In order to study problems without confinement, the implementation of periodic boundary conditions is a convenient route. In the presence of a temperature gradient the periodicity is obtained by defining a *cold* layer at one extreme of the simulation box and a *hot* layer in the center. In this way the simulation box is divided in two halves with increasing temperature towards the center, as has been sketched in Fig. 4.

Similar than in the presence of hard walls, there are different ways to enforce the cold and hot layers to have different temperatures than the bulk. One could consider the presence of virtual particles at fixed temperatures, or thermalize the particles in such layers. In fact, previous simulations with MPC and a temperature gradient have been very briefly reported by Pooley and Yeomans.[71] They employ a simulation box of size $L_z = 100$, and thermostat as the cold bath the layer between $z = 0$ and $z = 20$, and as the hot bath the layer between $z = 50$ and $z = 70$. They do not report any temperature jump although with the employed parameters we would expect them to be present.

Here we follow a different route in which the bath temperatures at the boundaries are not directly imposed, but a consequence of an energy flux. The original method was introduced by Hafskjold *et al.*[10] and employed in the first simulations with MD and temperature gradients.[73–75] They proposed to transfer fixed amounts of energy from the *cold* to the

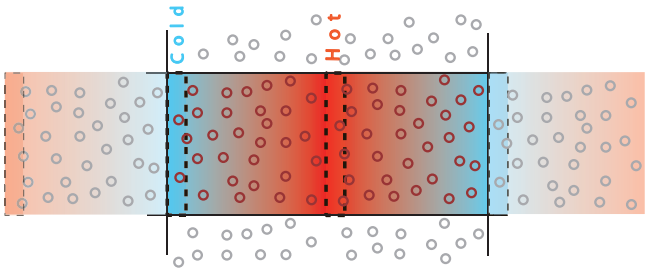

FIG. 4. Illustration of the periodic simulation box in the presence of a temperature gradient.

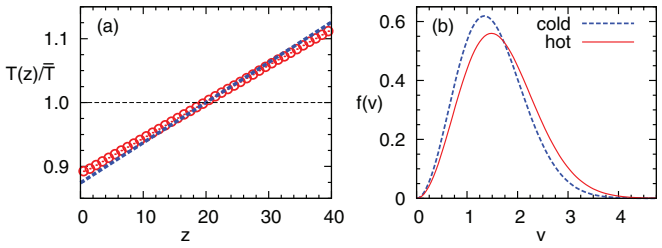

FIG. 5. (a) Temperature profile obtained from the velocity exchange algorithm with $h = 0.1$, $\alpha = 120$, and $\rho = 10$. Symbols correspond to the measured temperatures, dashed-line is the estimated temperature profile from Eq. (10). (b) Velocity squared distribution in Eq. (9) for the temperatures $T_c = 0.9$ and $T_h = 1.1$, typically used for the cold and hot baths.

hot layer. We employ the modification proposed by Müller-Plathe[11] and since then mostly employed with MD. The idea consists in determining the hottest particles in the cold slab and the coldest particles in the hot slab, and then exchange their velocities, as a type of a *Maxwell's demon*. This method has the advantage that the total energy E and momentum $\mathbf{P}$ of the system are exactly conserved. The temperature profile obtained with the velocity exchange algorithm in Fig. 5(a) shows a nice linear profile between the cold and hot slabs. This indicates that the velocity exchange algorithm provides a useful tool to study the effect of temperature gradients with open boundary conditions in combination with the MPC solvent. On the other hand, a temperature jump between the boundary layer and the bulk has been observed for some solvent parameters. Although now there are no walls implemented, in the boundary layers the average particle collision frequency is varied, and consequently the mean free path, what defines a corresponding Knudsen layer. For this case, we have not precisely quantified the effect but the observed trend is similar to before, namely, the temperature jump increases for small values of α and large values of h. Therefore, and also considering the artificial exchange of energy between the hot and cold slabs, these are usually disregarded from the analysis, similarly as it is done with the two previous boundary conditions.

In order to discuss how strong is the impact of such unphysical transformation, we characterize the distribution of particle velocity squared $f(v)$. In the presence of a temperature gradient the velocity distribution $P(\mathbf{v})$ can be approximated with Maxwell-Boltzmann, although strictly speaking it will deviate from it.[76] $f(v)$ can then be calculated as $f(v)dv = \int_\Omega v^2 P(\mathbf{v}) d\mathbf{v}$, where Ω denotes the integration over the polar and azimuthal angles,

$$f(v) = 4\pi \left(\frac{m}{2\pi k_B T}\right)^{3/2} v^2 \exp\left(-\frac{mv^2}{2k_B T}\right). \tag{9}$$

This is the so-called Maxwell's speed function. In Fig. 5(b), $f(v)$ is displayed for the two temperatures typically used as cold and hot baths. It can be observed that the difference between the two distributions is not so large, such that the exchange of velocity is easily absorbed by the new distribution. Additionally, the number of particles in each layer is large enough, such that the velocity distribution is not strongly perturbed. Although the energy flux is locally applied in each

exchange, the energy is distributed on average over the whole slab. As already discussed, for some parameters this velocity exchange is enough to produce a boundary temperature jump, and it will also then perturb the propagation of hydrodynamic interactions. The disruption is though not expected to be dramatic in the standard parameter regime since in each velocity exchange only a very small percentage of particles are affected. This artificial effect in the propagation of hydrodynamic interactions at the exchange layers has to be considered together with other three known coexisting effects. First are the standard finite size effects, this is the effect of the periodic images and more important the truncation of the hydrodynamic propagation spectra.[35] The third effect is the particular symmetry of these non-equilibrium simulations with the two subsequent temperature gradients in opposite directions. Consequently, it will be of particular importance to discuss the effect of the boundary layers in each application of the method.

The velocity exchange algorithm with both MD and MPC, controls the magnitude of the temperature gradient by tuning the time between velocity exchanges τ_{ex} and the number of particles n_{ex} in each exchange. To our knowledge, the determination of the temperature gradient as a function of the simulation parameters has only been quantified by performing the corresponding simulations. In the Appendix, we propose an argument by which the temperature gradient can be approximated by

$$|\nabla T| = \frac{1}{2}\frac{n_{ex}}{\tau_{ex}\kappa_T} k_B \overline{T} \frac{\ln(c\rho a A)}{A}, \tag{10}$$

with κ_T the thermal conductivity, $A = L_x L_y$ the cold/hot layer area, and the constant $c = 4\pi(m/2\pi k_B \overline{T})^{3/2}$. In Fig. 5(a) both simulated and estimated temperature profiles are displayed, showing that Eq. (10) gives a reasonable estimation of the temperature gradient. The deviation can be attributed to the number of approximations performed in calculating Eq. (10). In practice, the values of the temperature gradient, mean temperature, system size, and solvent parameters will be determined by the simulation requirements, and the exchange value τ_{ex}/n_{ex} will be estimated. The temperature gradient relaxes in between the velocity exchanges and since a stationary temperature profile is required, τ_{ex} is chosen as small as possible. It would, for example, not be reasonable to perform 100 exchanges every 100 steps instead of one exchange in every step.

IV. THERMAL DIFFUSIVITY

In a series of papers Ihle, Tüzel, and Kroll have studied in great detail the transport properties of the MPC solvent.[49,77–82] By using a discrete-time projection operator technique, they calculate Green-Kubo relations to characterize the MPC transport coefficients. The shear viscosity has been measured by them and others[50,79,80,83,84] showing in all cases very good agreement between analytical theory and simulation results for the whole range of MPC parameters. On the other hand, the simulation measurements of the self-diffusion coefficient show a noticeable discrepancy for the MPC parameter region where the Schmidt number is larger (small collision times h, and large rotation angle α).[50,51] This was attributed to the breakdown of the validity of the molecular chaos approximation employed in the theory. Molecular chaos assumes the absence of particle correlations, which are the origin of the building up of the hydrodynamic interactions.

Similar to other transport properties the analytical expression of the thermal diffusivity k_T can be expressed as the sum of a kinetic and a collision contribution $k_T = k_T^{kin} + k_T^{col}$ that read

$$\begin{aligned} k_T^{kin} &= \frac{k_B T h}{2m}\left[\frac{d}{1-cos(\alpha)} - 1 \right. \\ &\qquad \left. + \frac{2d}{\rho}\left(\frac{7-d}{5} - \frac{1}{4}\csc^2(\alpha/2)\right)\right], \\ k_T^{col} &= \frac{a^2}{h}\frac{1}{3(d+2)\rho}\left(1-\frac{1}{\rho}\right)[1-cos(\alpha)]. \end{aligned} \tag{11}$$

These expressions are valid for $d = 2$ or $d = 3$ dimensions. In previous works, k_T has been measured in equilibrium simulations by two types of measurements. One is performed by characterizing the dynamic structure factor, where information about thermal diffusivity and the sound attenuation is obtained.[79–82] Independent measurements of k_T are obtained by the quantification of the correlation of the entropy density. These values are in good agreement with the theoretical predictions, for the employed values of h. Alternatively, simulations in the presence of a temperature gradient have been reported by Pooley and Yeomans[71] in which measurements of k_T agree well with the analytical expressions for not too small values of the rotation angle α and the employed parameters.

In this work we obtain simulation measurements of the thermal diffusivity in a very broad range of parameters. These simulations are performed outside equilibrium, in the presence of steady temperature gradients induced with the three types of boundary conditions discussed in Sec. III. These results allow us to survey the accuracy of the analytical expressions where both, collisional and kinetic contributions, are simultaneously taken into account, and compare the performance of the different boundary conditions employed in this work. In the simulations, the energy exchange ΔE between the cold and the hot baths can be exactly quantified. ΔE is given by the difference of kinetic energies of the solvent before and after the contact with each heat bath. The energy exchange in the hot and the cold bath are exactly the same by construction in the case of the velocity exchange periodic boundary conditions. When the temperature gradient is simulated in combination with the walls, both quantities are not exactly the same, but only on average. The flux of energy $\mathbf{j}_q$ in the system is then obtained as

$$\mathbf{j}_q = \frac{\Delta E}{A\Delta t}, \tag{12}$$

with A the area, and Δt is the time interval considered to quantify ΔE. The *Fourier law* states that the heat flux is proportional to the negative temperature gradient,

$$\mathbf{j}_q = -\kappa_T \nabla T, \tag{13}$$

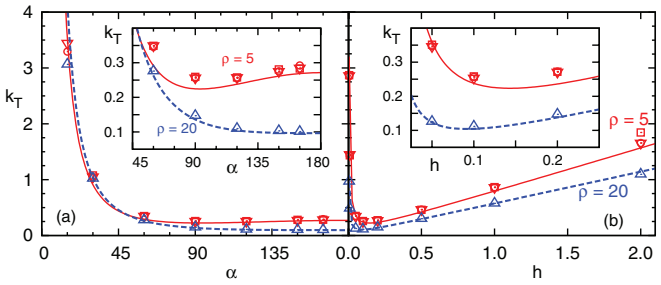

FIG. 6. Thermal diffusivity for two values of ρ. (a) k_T as a function of α for $h = 0.1$. (b) k_T as a function of h for $\alpha = 120$. The insets are a zoom-in for large values of α and small h, respectively. Lines correspond to the analytical approach in Eq. (11) and symbols to simulation results. Continuous lines correspond to $\rho = 5$ and dashes lines to $\rho = 20$. Triangles refer to simulations with walls and thermostats, circles to walls with virtual particles, and squares to the velocity exchange algorithm.

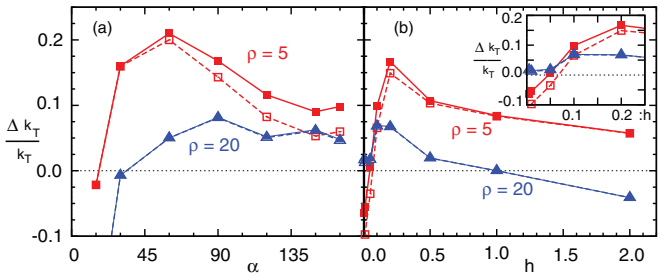

FIG. 7. Relative deviation of the simulated thermal diffusivity $k_{T,\,sim}$ with respect to the analytical approach $k_{T,\,an}$, $\Delta k_T/k_T \equiv (k_{T,\,sim} - k_{T,\,an})/k_{T,\,an}$ a) as a function of α (b) as a function of h. Simulation values are those presented in Fig. 6 for walls and thermostats. Open symbols and dashed lines employ both analytical contributions in Eq. (11), while solid symbols and solid lines take into account the collisional contribution in Eq. (15).

with κ_T the thermal conductivity, which is simply related to the thermal diffusivity k_T by

$$\kappa_T = \rho c_p k_T, \tag{14}$$

where c_p is the specific heat per particle at constant pressure, which is $c_p = (d+2)k_B/2$ since MPC describes an ideal fluid. The simulations have been performed with 10^5 time steps for equilibration and 10^5 time steps to obtain a good averaged value of ΔE. The simulation box is cubic with size $L = 40$ when using walls and doubled in the temperature gradient direction when employing the velocity exchange algorithm.

The thermal diffusivity k_T simulation results for two values of the number density ρ are displayed in Fig. 6 together with the corresponding analytical predictions in Eq. (11), as function of the rotation angle α and the collision time h. Comparison among the three temperature gradient implementations is performed for the smaller number density. The agreement is in general very good. Some deviations among the three sets of data can only be observed in the case of very large collision times, where the results obtained with the velocity exchange algorithm differ from the results obtained in the presence of the walls and the analytical results. From this we could conclude that the velocity exchange algorithm with periodic boundary conditions may display some artifacts when large collision times are employed. This could be related to the presence of periodic boundary conditions or to the velocity exchange algorithm. Nonetheless, in most applications the employed collision times are much smaller, such that this will in general not be a problem.

The accuracy of the analytical prediction in Eq. (11) is quantified more precisely in Fig. 7 by displaying the relative deviation of the simulated thermal diffusivity $k_{T,\,sim}$ with respect to the analytical approach $k_{T,\,an}$. Although the trend is not monotonous, it can be said that in general the prediction is better for systems with large ρ, large α, and large h. For small values of α and h the deviations decrease, probably due to a cancellation of errors. The analytical approach in Eq. (11) shows to underestimate the simulated values up to 8% for $\rho = 20$, but up to 20% for $\rho = 5$. Ihle *et al.* already reported in Ref. 81 that the expressions for the heat diffusivity in Eq. (11) were of $\mathcal{O}(1/\rho)$. In that work, higher order terms were calculated,

$$k_T^{col} = \frac{a^2}{h}\frac{1}{3(d+2)\rho}\left[1 + e^{-\rho}(\ln\rho - 1) - \frac{1}{\rho} - \frac{1}{\rho^2} + \mathcal{O}\left(\frac{1}{\rho^3}\right)\right][1 - cos(\alpha)]. \tag{15}$$

Figure 7 quantifies as well the relative deviation with respect to this expression. Equation (15) shows to worsen the prediction of Eq. (11) for $\rho = 5$ and not to change it appreciably for $\rho = 20$. The worsening could be explained since Eq. (15) is reported in Ref. 81 to be a better approach for large values of ρ.[85] Interestingly, the deviation shows to decrease significantly with increasing density, and for $\rho = 20$ it monotonously decreases with decreasing h. This could indicate that the origin of the deviations is a combination of two effects. One is the breakdown of the molecular chaos approximation, similar to what is already quantified for the self-diffusion coefficient.[51,82] And the other effect would be the influence of the density fluctuations at smaller densities. In a recent work,[86] Ihle derives the transport equations for MPC directly from the Liouville equation by means of a Chapman-Enskog expansion, where particle number fluctuations are automatically part of the derivation. This is in contrast with previous approximations where the particle number fluctuations were included by averaging over an assumed Poisson distribution of the particle positions. Unfortunately, quantitative comparison is not possible since only expressions in two dimensions and with a fixed collision angle $\alpha = 90^\circ$ are provided in that work. In spite of the deviations, the analytical values are reasonable, and the energy transport can be easily characterized within the MPC solvent.

V. DISCUSSION AND CONCLUSIONS

The implementation of temperature gradients with the MPC solvent in the presence of walls at fixed different temperatures results in the desired linear profiles. The temperatures at the walls show a temperature jump that depend on the Knudsen number and the boundary conditions, such that can be minimized by the use of adequate parameters. In case of open boundary conditions, the velocity exchange algorithm is

implemented. An argument to estimate the temperature gradient in terms of the exchange and simulation parameters valid for various simulation methods is presented and probed for MPC. The energy transport can be easily characterized within the MPC solvent, and shows to agree reasonably well with existing analytical values obtained by means of kinetic theory.

Another relevant aspect in the applicability of the method is the separation of the solvent characteristic times of energy and mass propagation. This is important when the system does not only contain linearly varying temperatures, but also more general temperature inhomogeneities. This is the case of a hot Brownian particle that carries with it a radially symmetric temperature distribution,[72,87,88] where a temperature drop at the particle surface has also been reported. For a spherical particle of radius σ, the characteristic thermal energy propagation time can be expressed as $\tau_k \sim \sigma^2/k_T$. The particle mass diffusion time is then $\tau_D \sim \sigma^2/D_s$, where the self-diffusion coefficient is $D_s \simeq k_B\overline{T}/6\pi\eta\sigma$ assuming the Stokes equation, stick boundary conditions, and being η the shear viscosity. In order to obtain an estimation of these characteristic times the transport coefficients can be safely approximated by the existing kinetic theory studies.[82] Parameters standardly employed in applications allow us to calculate $\tau_k/\tau_D \sim 10^{-2}$. This indicates that the important time scale separation can be properly taken into account by MPC, as already shown in the simulation of a thermophoretic nanoswimmer.[89] All these results put the MPC method forward as a promising and attractive tool to study mass and energy transport of soft matter systems in the presence of temperature inhomogeneities.

ACKNOWLEDGMENTS

The authors thank helpful discussions with Mingcheng Yang, Simone Wiegand, Andrea Costanzo, Eshan Irani, and Gerhard Gompper.

APPENDIX: RELATION BETWEEN THE EXCHANGE FREQUENCY AND THE TEMPERATURE GRADIENT IN THE VELOCITY EXCHANGE ALGORITHM

We following present an argument to obtain an estimation of the temperature gradient in terms of the exchange and simulation parameters. The temperature gradient ∇T is proportional to the heat flux $\mathbf{j}_q$ with the thermal conductivity κ_T as given in Eq. (13). The analytical expression of κ_T is in general known and for the MPC solvent has been discussed in Sec. IV. By definition the heat flux can be calculated with Eq. (12). Here, the time interval Δt is the time between exchanges τ_{ex}. The energy increment is given by the energy increment in each velocity exchange ΔE_{ex}, times the number of exchanges n_{ex}, and divided by 2 since the energy flux is distributed in the two half boxes; this is

$$\Delta E = \frac{1}{2} n_{ex} \Delta E_{ex}. \tag{A1}$$

The energy increment in each velocity exchange is

$$\Delta E_{ex} = \frac{1}{2} m \left(v_{min}^2 - v_{max}^2 \right), \tag{A2}$$

v_{min} corresponds to the coldest particle in the hot slab. In general, we can approximate $v_{min} \simeq 0$, as can be seen in Fig. 5(b). v_{max} corresponds to the hottest particle in the cold slab. In order to get a rough estimation of such velocity in terms of the input parameters, we first approximate the temperature $T_c \simeq \overline{T}$ in Eq. (9). Second, since we are in the tail of the distribution, we neglect the correction given by the factor v_{max}^2 in Eq. (9), such that

$$f(v_{max}) \simeq c \exp\left(-\frac{m v_{max}^2}{2 k_B \overline{T}} \right). \tag{A3}$$

And third we assume that in such a cold layer there are $\rho a A$ particles, or similarly that the density is the same as the average density $\rho_c \simeq \rho$, and that there will always be at least one particle with the temperature at the tail of the distribution,

$$f(v_{max}) \simeq \frac{1}{\rho a A}. \tag{A4}$$

From Eqs. (A3) and (A4), we obtain our rough estimation of v_{max},

$$v_{max}^2 \simeq \frac{2 k_B \overline{T}}{m} \ln(c \rho a A). \tag{A5}$$

Therefore, comparing the heat flux $\mathbf{j}_q$ in Eqs. (12) and (13), and substituting Eq. (A5) in Eq. (A2) and then in Eq. (A1), we get that Eq. (10) provides the estimated temperature gradient.

The resulting expression in Eq. (10) is expected to be valid for simulations with the MPC solvent, and also with pure MD, or any other technique that employs the velocity exchange algorithm, with a understood then as the thickness of the cold/hot layer.

[1] J. Giddings, Science **260**, 1456 (1993).
[2] D. Vigolo, R. Rusconi, H. A. Stone, and R. Piazza, Soft Matter **6**, 3489 (2010).
[3] S. Duhr and D. Braun, Proc. Natl. Acad. Sci. U.S.A. **103**, 19678 (2006).
[4] H. R. Jiang, H. Wada, N. Yoshinaga, and M. Sano, Phys. Rev. Lett. **102**, 208301 (2009).
[5] P. Baaske, F. M. Weinert, S. Duhr, K. H. Lemke, M. J. Russell, and D. Braun, Proc. Natl. Acad. Sci. U.S.A. **104**, 9346 (2007).
[6] I. Budin, R. J. Bruckner, and J. W. Szostak, J. Am. Chem. Soc. **131**, 9628 (2009).
[7] S. Wiegand, J. Phys.: Condens. Matter **16**, R357 (2004).
[8] J. K. G. Dhont, J. Chem. Phys. **120**, 1632 (2004).
[9] A. Würger, Rep. Prog. Phys. **73**, 126601 (2010).
[10] B. Hafskjold, T. Ikeshoji, and S. K. Ratkje, Mol. Phys. **80**, 1389 (1993).
[11] F. Müller-Plathe, J. Chem. Phys. **106**, 6082 (1997).
[12] M. Vladkov and J.-L. Barrat, Nano Lett. **6**, 1224 (2006).
[13] D. Reith and F. Müller-Plathe, J. Chem. Phys. **112**, 2436 (2000).
[14] P. Polyakov, F. Müller-Plathe, and S. Wiegand, J. Phys. Chem. B **112**, 14999 (2008).
[15] B. Rousseau, C. Nieto-Draghi, and J. Bonet Avalos, Europhys. Lett. **67**, 976 (2004).
[16] G. A. Bird, *Molecular Gas Dynamics and the Direct Simulation of Gas Flows* (Clarendon, Oxford, 1994).
[17] M. A. Gallis, J. R. Torczynski, and D. J. Rader, Phys. Fluids **13**, 3482 (2001).
[18] W. W. Liou and Y. Fang, J. Microelectromechan. Syst. **10**, 274 (2001).
[19] *Novel Methods in Soft Matter Simulations*, edited by M. Karttunen, I. Vattulainen, and A. Lukkarinen (Springer, New York, 2004).
[20] G. R. McNamara and G. Zanetti, Phys. Rev. Lett. **61**, 2332 (1988).
[21] S. Succi, *The Lattice Boltzmann Equation: For Fluid Dynamics and Beyond* (Clarendon, Oxford, 2001).
[22] P. J. Hoogerbrugge and J. M. V. A. Koelman, Europhys. Lett. **19**, 155 (1992).
[23] P. Español and P. Warren, Europhys. Lett. **30**, 191 (1995).

[24]R. D. Groot and P. B. Warren, J. Chem. Phys. **107**, 4423 (1997).
[25]F. J. Alexander, S. Chen, and J. D. Sterling, Phys. Rev. E **47**, 2249(R) (1993).
[26]P. Lallemand and L.-S. Luo, Phys. Rev. E **68**, 036706 (2003).
[27]M. Watari and M. Tsutahara, Phys. Rev. E **67**, 036306 (2003).
[28]N. I. Prasianakis and I. V. Karlin, Phys. Rev. E **76**, 016702 (2007).
[29]G. Gonnella, A. Lamura, A. Piscitelli, and A. Tiribocchi, Phys. Rev. E **82**, 046302 (2010).
[30]A. Scagliarini, L. Biferale, M. Sbragaglia, K. Sugiyama, and F. Toschi, Phys. Fluids **22**, 055101 (2010).
[31]P. Español, Europhys. Lett. **40**, 631 (1997).
[32]J. Bonet-Avalós and A. D. Mackie, Europhys. Lett. **40**, 141 (1997).
[33]M. Ripoll, P. Español, and M. H. Ernst, Int. J. Mod. Phys. C **9**, 1329 (1998).
[34]M. Ripoll and M. H. Ernst, Phys. Rev. E **71**, 041104 (2005).
[35]M. Ripoll and M. H. Ernst, Phys. Rev. E **72**, 011101 (2005).
[36]J. Bonet-Avalós and A. D. Mackie, J. Chem. Phys. **111**, 5267 (1999).
[37]A. D. Mackie, J. Bonet-Avalós, and V. Navas, Phys. Chem. Chem. Phys. **1**, 2039 (1999).
[38]P. Nikunen, M. Karttunen, and I. Vattulainen, Comput. Phys. Commun. **153**, 407 (2003).
[39]G. D. Fabritiis, M. Serrano, P. Español, and P. V. Coveney, Physica A **361**, 429 (2006).
[40]L. Pastewka, D. Kauzlarić, A. Greiner, and J. G. Korvink, Phys. Rev. E **73**, 037701 (2006).
[41]E. Abu-Nada, Phys. Rev. E **81**, 056704 (2010).
[42]A. Chaudhri and J. R. Lukes, ASME Trans. J. Heat Transfer **131**, 033108 (2009).
[43]R. Qiao and P. He, Mol. Simul. **33**, 677 (2007).
[44]A. Malevanets and R. Kapral, J. Chem. Phys. **110**, 8605 (1999).
[45]A. Malevanets and R. Kapral, J. Chem. Phys. **112**, 7260 (2000).
[46]D. Lüsebrink, Ph.D. dissertation (Cologne University, Cologne, Germany, 2011).
[47]R. Kapral, Adv. Chem. Phys. **140**, 89 (2008).
[48]G. Gompper, T. Ihle, D. M. Kroll, and R. G. Winkler, Adv. Polym. Sci. **221**, 1 (2009).
[49]T. Ihle and D. M. Kroll, Phys. Rev. E **63**, 020201(R) (2001).
[50]M. Ripoll, K. Mussawisade, R. G. Winkler, and G. Gompper, Europhys. Lett. **68**, 106 (2004).
[51]M. Ripoll, K. Mussawisade, R. G. Winkler, and G. Gompper, Phys. Rev. E **72**, 016701 (2005).
[52]H. Noguchi, N. Kikuchi, and G. Gompper, Europhys. Lett. **78**, 10005 (2007).
[53]I. O. Götze, H. Noguchi, and G. Gompper, Phys. Rev. E **76**, 046705 (2007).
[54]K. Mussawisade, M. Ripoll, R. G. Winkler, and G. Gompper, J. Chem. Phys. **123**, 144905 (2005).
[55]M. Belushkin, R. Livi, and G. Foffi, Phys. Rev. Lett. **106**, 210601 (2011).
[56]J. T. Padding and A. A. Louis, Phys. Rev. Lett. **93**, 220601 (2004).
[57]A. Wysocki, C. P. Royall, R. G. Winkler, G. Gompper, H. Tanaka, A. van Blaaderen, and H. Löwen, Soft Matter **5**, 1340 (2009).
[58]M. Ripoll, P. Holmqvist, R. G. Winkler, G. Gompper, J. K. G. Dhont, and M. P. Lettinga, Phys. Rev. Lett. **101**, 168302 (2008).
[59]M. Ripoll, Phys. Rev. E **83**, 040701(R) (2011).
[60]S. Frank and R. G. Winkler, Europhys. Lett. **83**, 38004 (2008).
[61]G. Rückner and R. Kapral, Phys. Rev. Lett. **98**, 150603 (2007).
[62]J. Elgeti, U. B. Kaupp, and G. Gompper, Biophys. J. **99**, 1018 (2010).
[63]I. O. Götze and G. Gompper, Phys. Rev. E **82**, 041921 (2010).
[64]A. Lamura, G. Gompper, T. Ihle, and D. M. Kroll, Europhys. Lett. **56**, 319 (2001).
[65]A. Lamura and G. Gompper, Eur. Phys. J. E **9**, 477 (2002).
[66]H. Noguchi and G. Gompper, Proc. Natl. Acad. Sci. U.S.A. **102**, 14159 (2005).
[67]M. Smoluchowski, Ann. Phys. **300**, 101 (1898).
[68]A. Beskok and G. E. Karniadakis, J. Thermophys. Heat Transf. **8**, 647 (1994).
[69]Y. H. Zhang, X. J. Gu, R. W. Barber, and D. R. Emerson, EPL **77**, 30003 (2007).
[70]L. Zheng, Z. L. Guo, and B. C. Shi, EPL **82**, 44002 (2008).
[71]C. M. Pooley and J. M. Yeomans, J. Phys. Chem. B **109**, 6505 (2005).
[72]S. Merabia, S. Shenogin, L. Joly, P. Keblinski, and J. L. Barrat, Proc. Natl. Acad. Sci. U.S.A. **106**, 15113 (2009).
[73]J. Kincaid and B. Hafskjold, Mol. Phys. **82**, 1099 (1994).
[74]B. Hafskjold and S. K. Ratkje, J. Stat. Phys. **78**, 463 (1995).
[75]B. Hafskjold, I. Fujihara, and T. Ikeshoji, Mol. Phys. **90**, 999 (1997).
[76]E. Bringuier and A. Bourdon, Physica A **385**, 9 (2007).
[77]T. Ihle and D. M. Kroll, Phys. Rev. E **67**, 066705 (2003).
[78]E. Tüzel, M. Strauss, T. Ihle, and D. M. Kroll, Phys. Rev. E **68**, 036701 (2003).
[79]T. Ihle and D. M. Kroll, Phys. Rev. E **67**, 066706 (2003).
[80]T. Ihle, E. Tüzel, and D. M. Kroll, Phys. Rev. E **70**, 035701(R) (2004).
[81]T. Ihle, E. Tüzel, and D. M. Kroll, Phys. Rev. E **72**, 046707 (2005).
[82]E. Tüzel, T. Ihle, and D. M. Kroll, Phys. Rev. E **74**, 056702 (2006).
[83]N. Kikuchi, C. M. Pooley, J. F. Ryder, and J. M. Yeomans, J. Chem. Phys. **119**, 6388 (2003).
[84]R. G. Winkler and C.-C. Huang, J. Chem. Phys. **130**, 074907 (2009).
[85]An alternative expression for k_T^{col} is provided in Ref. 81 valid for small values of ρ. Such expression is though problematic since the observed deviations become up to 200% large. It could be that the expression is only valid for $\rho \ll 1$, what would be a very unusual limit for MPC, or more likely just contain a misprint.
[86]T. Ihle, Phys. Chem. Chem. Phys. **11**, 9667 (2009).
[87]D. Rings, R. Schachoff, M. Selmke, F. Cichos, and K. Kroy, Phys. Rev. Lett. **105**, 090604 (2010).
[88]L. Joly, S. Merabia, and J. L. Barrat, Europhys. Lett. **94**, 50007 (2011).
[89]M. Yang and M. Ripoll, Phys. Rev. E **84**, 061401 (2011).